Proc. Natl. Acad. Sci. USA
Vol. 93, pp. 8846–8851, August 1996
Biochemistry

A structure-based catalytic mechanism for the xanthine oxidase family of molybdenum enzymes

ROBERT HUBER*†, PETER HOF*, RUI O. DUARTE‡, JOSE J. G. MOURA‡, ISABEL MOURA‡, MING-YIH LIU§, JEAN LEGALL§, RUSS HILLE¶, MARGARIDA ARCHER‖, AND MARIA J. ROMÃO‖

*Max-Planck-Institut für Biochemie, D-82152 Martinsried, Germany; ‖Instituto de Tecnologia Química e Biológica, Rua da Quinta Grande, Apartado 127, 2780 Oeiras and Instituto Superior Técnico, Departamento de Química, 1096 Lisboa Codex, Portugal; ‡Departamento de Química (and Centro de Química Fisica Biológica) Faculdade de Ciências e Tecnologia, Universidade Nova de Lisboa, 2825 Monte de Caparica, Portugal; §Department of Biochemistry and Molecular Biology, University of Georgia, Athens, GA 30602; and ¶Department of Medical Biochemistry, Ohio State University, Columbus, OH 43210-1218

Contributed by Robert Huber, April 12, 1996

ABSTRACT **The crystal structure of the xanthine oxidase-related molybdenum-iron protein aldehyde oxido-reductase from the sulfate reducing anaerobic Gram-negative bacterium *Desulfovibrio gigas* (Mop) was analyzed in its desulfo-, sulfo-, oxidized, reduced, and alcohol-bound forms at 1.8-Å resolution. In the sulfo-form the molybdenum molybdopterin cytosine dinucleotide cofactor has a dithiolene-bound fac-[Mo, =O, =S, ---(OH2)] substructure. Bound inhibitory isopropanol in the inner compartment of the substrate binding tunnel is a model for the Michaelis complex of the reaction with aldehydes (H—C=O, —R). The reaction is proposed to proceed by transfer of the molybdenum-bound water molecule as OH— after proton transfer to Glu-869 to the carbonyl carbon of the substrate in concert with hydride transfer to the sulfido group to generate [MoIV, =O, —SH, ---(O—C=O, —R)). Dissociation of the carboxylic acid product may be facilitated by transient binding of Glu-869 to the molybdenum. The metal-bound water is replenished from a chain of internal water molecules. A second alcohol binding site in the spacious outer compartment may cause the strong substrate inhibition observed. This compartment is the putative binding site of large inhibitors of xanthine oxidase.**

Molybdenum containing hydroxylases catalyze the incorporation of oxygen derived from water into substrates in a manner whereby reducing equivalents are generated rather than consumed (1–3). The molybdenum is associated with a pterin derivative, called molybdopterin, to form the molybdenum cofactor (Mo-co). Xanthine oxidase, a representative member of this group of enzymes, contains Mo-co and, as additional redox centers, two (2Fe–2S) iron-sulfur clusters and a flavin. On the basis of a variety of spectroscopic techniques, mechanisms for the hydroxylation reaction have been proposed but have suffered from the lack of comprehensive structural data. The aldehyde oxido-reductase from the sulfate reducing anaerobic bacterium *Desulfovibrio gigas* (Mop) is a member of the xanthine oxidase protein family (4), and its crystal structure has been analyzed at 2.25-Å resolution (5). Mop, a homodimer of 907 amino acid residues, catalyzes the oxidation of aldehydes to carboxylic acids. The pterin cofactor in Mop is a molybdopterin cytosine dinucleotide. It has two (2Fe–2S) centers but lacks the flavin domain. The protein molecule is folded into four domains, of which the first two bind the iron sulfur clusters and the others are associated with Mo-co. Mo-co is deeply buried in the protein accessible through a 15-Å-deep tunnel (Fig. 1). The molybdenum is pentacoordinated with two dithiolene sulfur atoms of the molybdopterin and three oxygen ligands, of which one is presumably an oxo and one a sulfido group in the functional sulfo-form of the enzyme in analogy to xanthine oxidase. In an effort to define the metal coordination and its role in catalysis more precisely we extended the crystallographic analysis to the desulfo-, sulfo-, oxidized, reduced, and alcohol-bound forms of the enzyme at 1.8-Å resolution, from which we derive a mechanism for the hydroxylation reaction of Mop and the xantine oxidase family in general.

EXPERIMENTAL PROCEDURES

Mop protein had been prepared in an anaerobic chamber under an atmosphere containing 5% hydrogen/95% nitrogen. The purification steps were essentially as described (6), with the notable exception that Mop behaved as a more acidic protein than in aerobic conditions and was found, after elution from the first DEAE cellulose column, together with the flavodoxin-containing fraction. Because Mop was separated from hydrogenase and intermediate electron carriers, it was slowly reoxidized as evidenced by the reappearance of its red color due to its (2Fe–2S) centers. Once fully purified, Mop was distributed in sealded small containers, immediately frozen in liquid nitrogen, and stored at −80°C until utilization. Crystallization was carried out using solvents and conditions as described (6), but was conducted under argon. The ANE data set was measured from crystals mounted in capillaries under argon. Other crystals were exposed to air and used for various soaking experiments that were carried out in sealed vessels. The soaking conditions are reported in Table 1. X-ray diffraction data were collected at −17°C in a cold stream of air with a Mar Research imaging plate system (Hamburg, Germany) installed on a Rigaku rotating anode generator and evaluated with MOSFLM (7) and CCP4 (8). The crystal structures were refined with X-PLOR (9) using the Engh and Huber geometric and force field parameter set (10) and inspected with FRODO (11). The diffraction data were usually measured from one crystal except with ANE from two crystals (Table 1). Protocols were chosen with the aim to establish reduction, inhibitor-binding, product-binding, substrate-binding, and resulfuration. Data sets were obtained with reduced (RED, SRED, SPVM), resulfurated (SRED, SPVM, SVPP, SBEN, SASX, SOXY, SOX3), and inhibitor-bound (ANE, SVPP, SBEN, SASX) enzyme under the experimental conditions summarized in Table 1. The concentration of reagents used was very high to ensure reaction in the crystalline state, but pH and redox state were difficult to control under these conditions and we were

The publication costs of this article were defrayed in part by page charge payment. This article must therefore be hereby marked "*advertisement*" in accordance with 18 U.S.C. §1734 solely to indicate this fact.

Abbreviations: EPR, electron paramagnetic resonance, EXAFS, extended x-ray absorption fine structure, PEG, polyethylene glycol; Mo-co, molybdenum cofactor; Mop, molybdenum-iron protein aldehyde oxido-reductase from *Desulfovibrio gigas*.

Data deposition: The atomic coordinates and structure factors have been deposited in the Protein Data Bank, Brookhaven National Laboratory, Upton, NY 11973 (reference T7184; ID code, 1ALO). This information is embargoed until November 17, 1996.

†To whom reprint requests should be addressed.

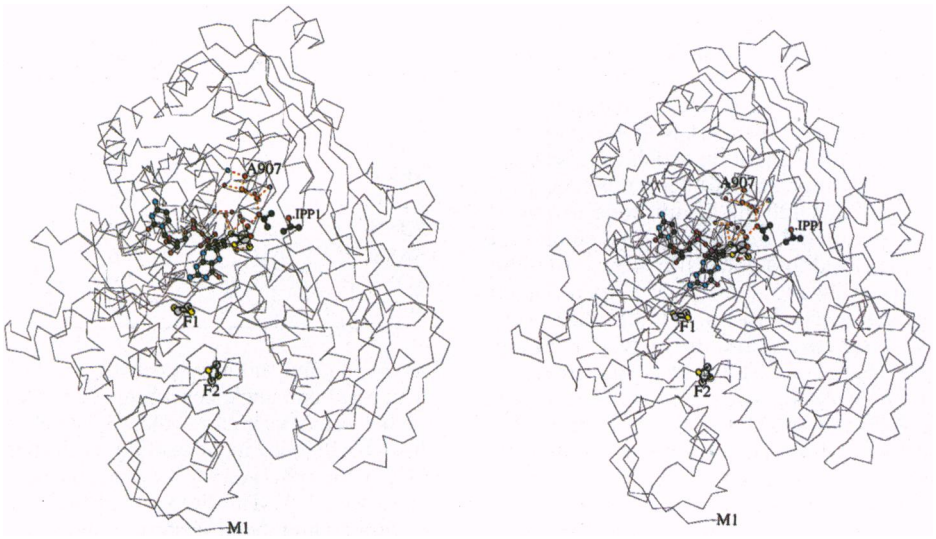

FIG. 1. C^{α} chain tracing of a subunit of Mop with the Mo-co, the two iron sulfur clusters, F1 and F2, and the outer isopropanol ligand, IPP1, and the N and C termini Met-1 and Ala-907 highlighted. The view is from a direction identical to Fig. 4.

limited in choice of the reducing agents by solubility in the harvesting buffer and sensitivity of the crystals. pH and redox potentials were directly measured in the soaking solutions after the crystals had been removed and mounted and are reported in Table 1 without corrections.

RESULTS

Spectroscopic data in solution showed that dithiothreitol, the reducing agent mostly employed, bleaches Mop's visible absorption by about 60% compared with 68% with dithionite. According to the measured redox potentials of the soaking solutions (Table 1) compared with the reported mid point redox potentials of the molybdenum in Mop (12), we presume that all derivatives except ANE and SOX3 are reduced to various degrees, to the greatest extent, in RED, SRED, and SPVM. RED was measured in a cell under carbon monoxide pressurized at 5 atmospheres to avoid dioxygen contamination. The SVPP, SPVM, and SBEN derivatives were prepared under conditions where (partial) resulfuration occurs in xanthine oxidase in the presence of sulfide (13–15). Pyrrole-2-aldehyde and vanilline were included to the reaction mix as possible oxo acceptors and 2-methylpyridine-*N*-oxide as oxo donor. However, resulfuration was also achieved by sulfide treatment alone as evident in the SRED and SASX data sets. Resulfuration occurred under alkaline conditiones; unfortunately the crystals cracked after transfer to neutral pH, where the

Table 1. Collection of data and statistics of structure determination and refinement

Data set	Total/unique reflections	R_s*	Resolution, Å	Completeness, %	$\langle I\rangle/\langle\sigma I\rangle$, last shell	Model *R*-factor,† %	Last shell	Resolution, Å	rms bond,‡ Å	rms angle,‡ degree
ANE	537,957/66,283	0.096	2.0	99.5	10.0–2.5	17.84	27.55	10-2.0	0.009	1.81
RED	369,271/58,791	0.151	2.0	88.3	7.0–2.2	18.13	28.06	10-2.0	0.009	1.77
SRED	236,604/71,543	0.103	1.95	95.7	3.3–1.5	19.01	36.1	10-1.95	0.009	1.78
SVPP	279,437/76,304	0.089	1.9	97.5	3.5–2.0	19.01	36.09	10-1.9	0.009	1.78
SPVM	353,460/88,714	0.094	1.8	95.9	4.5–3.5	19.19	34.62	10-1.8	0.009	1.78
SBEN	171,398/80,531	0.069	1.8	87.7	3.7–2.5	19.19	34.18	10-1.8	0.010	1.78
SASX	323,776/91,158	0.079	1.8	98.1	5.0–2.0	19.40	34.23	10-1.8	0.009	1.79
SOXY	405,807/93,219	0.090	1.78	97.6	3.5–1.5	19.56	37.4	10-1.78	0.009	1.79
SOX3	418,807/82,854	0.106	1.86	98.2	3.0–1.2	19.52	36.0	10-1.85	0.009	1.80

Note: number of protein atoms = 7367; number of solvent atoms = 498

*$R_s = \Sigma(I - \langle I\rangle)/\Sigma\ (I)$; measured intensity, $\langle I\rangle$ averaged value; the summation is over all measurements.

†Data are for the start and end of the data collection.

‡The root mean square (rms) deviations from ideal values; E, redox potentials of the crystal soaking solutions as measured with a Pt/Ag/AgCl electrode (Metrohm, Herisau).

The harvesting buffer (hb) is as follows: 0.2 M Hepes/0.2 M $MgCl_2$/30% PEG 4000/30% isopropanol, pH 7.2; polyethylene g kol (PEG) buffer: the same without isopropanol. The data sets are as follows. ANE, anaerobically (AE) prepared material, crystal kept under argon in hb, pH 6.8. RED, AE material; crystals in hb under air; soaked over night in hb with 50 mM dithiothreitol, 100 mM tributhylphosphine, pH 6.9; E, −370 mV; crystal mounted under carbon monoxide and measured at 5 atmospheres pressure. SRED, AE material; PEG buffer with 50 mM Na_2S, 50 mM Na_2SO_3 overnight, then added 50 mM dithiothreitol, and 50 mM tributylphosphine for 2 h, pH 8.2; E, −425 mV. SVPP, AE material, crystals in hb with 60 mM Na_2S, 50 mM vanilline, 50 mM pyrrole-2-aldehyde, 50 mM 2-methyl pyridine-*N*-oxide, pH 7.5; E, −255 mV. SPVM, AE material, PEG buffer with 60 mM Na_2S, 20 mM dithiothreitol, 20 mM vanilline, 50 mM pyrrole-2-aldehyde, 50 mM 2-methyl pyridine-*N*-oxide, pH 8.6, E, −440 mV. SBEN, AE material, PEG buffer under resulfuration conditions as with SPVM overnight, then transferred in PEG buffer with 50 mM Na_2S, 100 mM benzyl alcohol for 5 h, pH 7.2; E, −95 mV. SASX, AE material; PEG buffer with 50 mM Na_2S, 50 mM Na meta arsenite, saturated xanthine, pH 8.8; E, −30 mV.

SOXY, AE material sulfurated as SRED, then transferred in PEG buffer with Tris, triethanolamine, pH 8.5 for 4 h; E, −280 mV. SOX3, AE material sulfurated as SRED, then transferred in PEG buffer with Tris, triethanolamine, ferricyanide, pH 8.4 for 5 h. E, +235 mV.

&Rs=Σ(I−⟨I⟩)/Σ(I), measured intensity, ⟨I⟩ averaged value; the summation is over all measurements;

§The rms deviations from ideal values; E, redox potentials of the crystal soaking solutions as measured with a Pt/Ag/ACCl electrode (Metrohm, Herisau).

oxo-forms ANE and RED had been measured. But resulfurated crystals could be transferred into sulfide-free buffer at alkaline pH under slightly reducing (SOXY) and strongly oxidizing conditions (SOX3).

The diffraction data showed variation in the unit cell dimensions between the various derivatives. Refinement began therefore with a rigid body refinement, in which the *R*-factors fell by ≈20%. The molybdenum site had been modeled with penta-coordinate molybdenum and the ligands were arranged in a distorted square pyramidal geometry. The equatorial plane was defined by the two dithiolene sulfur atoms from the cofactor and two oxygen ligands. A third oxygen ligand occupied the apical position. The Mo—S, —O distances were set to 2.4 Å and 1.8 Å, respectively, and the molybdenum was positioned in the equatorial plane (5). In the crystal structure analysis and refinement of ANE, which was measured first, three oxygen ligands of the molybdenum were seen. No significant difference was observed to data sets obtained previously from crystals that had been prepared aerobically. The atomic positions were restrained to the geometry above but positive density appeared in difference Fourier maps between the two oxygens, MOH1 and MOH3, and the molybdenum, which disappeared when the bond lengths were adjusted to 1.6 Å. A longer bond from the metal was required for the oxygen ligand trans to S7′, MOH2. To quantitate other possible significant differences at the molybdenum site, atomic positions were read from the maps of all derivatives for MOH1, MOH2, and MOH3, and their distances to the molybdenum were measured (Fig. 2) and Table 2.

The uncertainty of these values is considerable and the differences seen between the derivatives for MOH2 and MOH1 are probably insignificant. The Mo—MOH3 bond lengthening in RED is probably significant, however, and the much longer bonds in the S (sulfurated) derivatives are certainly so. The molybdenum clearly deviates from the equatorial plane and is shifted toward the apical ligand by about 0.4–0.7 Å for the more reduced derivatives (Fig. 2). More structural differences between the (partially) oxidized forms and the more reduced forms RED, SRED, and SPVM were observed in that the latter have a wider separation of the dithiolene sulfurs (3.5 Å compared with 3.0 Å) and a considerable puckering of the dithiolene molybdenum cycle. They also have a density bridge between Glu-869 $O^{\varepsilon 1}$ and MOH2, indicating a shorter (hydrogen-) bond distance.

The electron density also showed a large increase in size and substantial bond lengthening of the apical MOH3 ligand in the sulfido derivatives, as expected for exchange of sulfur for oxygen. Consequently, sulfur was put in the crystallographic calculations and refined. Its temperature factor was equal or marginally higher compared with the other molybdenum ligands, suggesting almost complete replacement. For the refinement calculations the molybdenum ligands were modeled for the nine derivatives with Mo—MOH1 bonds of 1.6 Å and Mo—MOH2 bonds of 2.2 Å. The Mo—MOH3 bond was modeled with 1.6 Å for ANE, 1.9 Å for RED, and 2.2 Å for the sulfido derivatives. MOH3 was put in

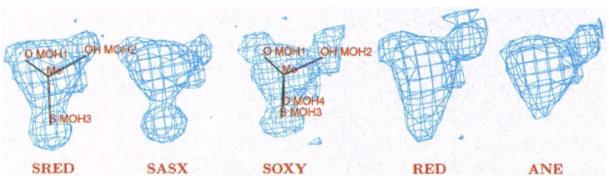

FIG. 2. Gallery of electron densities at the molybdenum and its three ligands MOH1, MOH2, MOH3 of SRED; SASX, reduced and partly oxidized sulfo-forms; SOXY, a partly hydrolyzed and oxidized sulfo-form; and of RED, ANE, reduced and oxidized desulfo-forms. MOH1 is an oxo ligand, MOH2 a water molecule, and MOH3 a sulfido or oxo group, respectively. The view is from the molybdenum toward the dithiolene group. 2Fo–Fc maps are contoured at 0.9 σ.

Table 2. Distances of the molybdenum to its ligands as read from the electron density maps

	MOH2, Å	MOH1, Å	MOH3, Å	MOH4, Å
ANE	2.5	1.5	1.6	
RED	2.5	1.9	2.1	
SRED	2.3	1.6	2.5	
SPVM	2.3	1.6	2.3	
SVPP	2.2	2.0	2.4	
SBEN	2.1	1.9	2.4	
SASX	2.2	1.6	2.4	
SOXY	2.3	1.9	2.2	1.6
SOX3	2.3	1.6	2.2	1.6

as oxygen and sulfur, respectively, in the two sets of derivatives. The bond and angle constraints of the Mo group had only 10% of the usual weights to allow relatively free movement of the ligands. Indeed, in all sulfido derivatives, except SOXY and SOX3, the observed Mo—S bond as measured from the maps is close to 2.4 Å. The SOXY and SOX3 crystals that were first sulfurated and then transferred into sufide-free buffer showed a rapid loss of the sulfido group and its replacement by an oxo atom. The density was satisfactorily modelled with half occupied sulfur (MOH3) and oxygen (MOH4) atoms at distances of 2.2 Å and 1.6 Å, respectively.

In SVPP and ANE an electron density with the shape of a tripod is very well defined (IPP3 in Fig. 3) and was modeled as an isopropanol molecule. A second equally well-defined isopropanol molecule (IPP1) is located further up toward the entrance of the substrate tunnel (Fig. 4), which forms a dish-shaped depression on the protein surface. A third isopropanol (IPP4) is bound there. Crystals in PEG buffer without isopropanol show unidentified, very voluminous electron densities in this wide, solvent accessible cavity defining it as a general ligand binding site. It is located in the back of the molecule and marked by the IPP1 ligand in Fig. 1. SBEN has a much larger density at the IPP3 site, which can be fitted by a benzyl alcohol molecule with the aromatic moiety coplanar with Tyr-535. SASX has the IPP3 site filled with a tripod density probably representing incompletely occupied arsenite.

The (2Fe–2S) iron-sulfur centers are unchanged between the various derivatives. Some structural differences are seen with three magnesium binding sites, identified in the more highly resolved crystallographic analysis described here, and the side chain of Cys-661, which has two alternative conformations in SVPP, probably in response to binding of an isopropanol molecule close by. These sites are far from the molybdenum and presumably insignificant for the enzymatic reaction.

DISCUSSION

Mop and xanthine oxidase are structurally related as documented by the conservation of the amino acid sequences in general and of the protein segments at the molybdenum and iron cofactors in particular (5). In addition, the ability of xanthine oxidase to utilize a wide range of aldehydes as substrate is well documented, so that there is also a significant functional relationship between the two enzymes (16, 17). Furthermore, studies of structural and spectroscopic properties of the metal cofactors of both enzymes indicated a close similarity (17, 18). Particularly significant is the observation that the molybdenum centers of Mop and xanthine oxidase exhibit very similar electron paramagnetic resonance (EPR) properties (17). This justifies interpretation of the wealth of functional and spectroscopic data of the metal sites of xanthine oxidase on the basis of the Mop structure.

A penta-coordinate geometry as observed in Mop is quite common for molybdenum IV,V complexes with sulfur, oxygen, and nitrogen ligands. The metal is generally displaced from the equatorial plane toward the apical ligand. MoVI complexes, on the other hand, are usually hexa-coordinate; the penta-

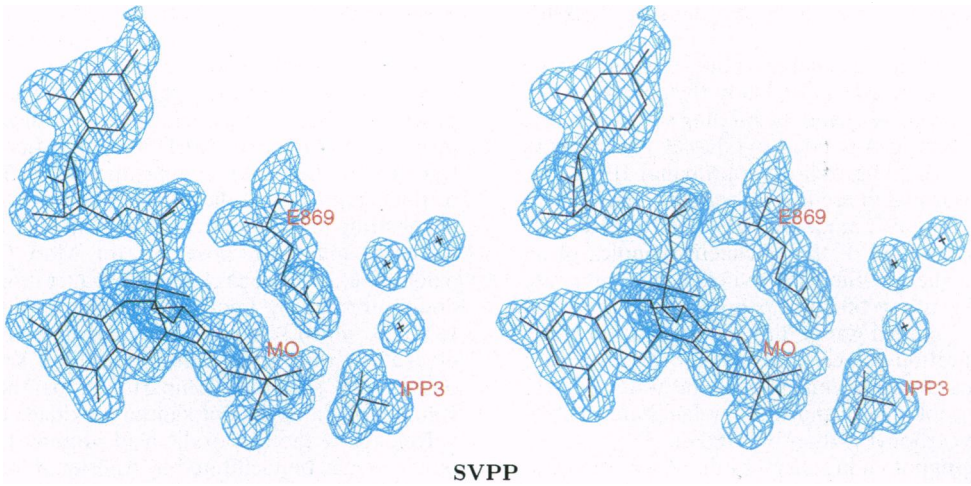

FIG. 3. Electron density contoured at 0.9 σ of the 2Fo–Fc map of SVPP showing the molybdenum molybdopterin cytosine dinucleotide with the associated metal ligands, the Glu-869, the inner isopropanol (IPP3), and the three internal water molecules. The orientation is identical to Fig. 5 and similar to Fig. 4, where atom labels and identifications are given [produced with FRODO (11)].

coordinate molybdenum in the oxidized state is poised toward the lower oxidation number. In small molecule structures Mo═O distances show a narrow distribution centered at 1.7 Å. Mo-H_2O has a broad distribution between 2.1 Å and 2.4 Å, with a mean of 2.2 Å. Mo-OH, with few observations, shows a mean value of 1.9 Å. MOH2 is therefore most likely a coordinated water molecule in all derivatives. MOH1 is identified as an oxo group by its short distance to the molybdenum and the absence of any hydrogen bonding interaction with protein groups. The sulfuration experiments identified MOH3 as the sulfido group. MOH3 is an oxo group in ANE, but moved to a somewhat longer distance upon reduction in RED, as expected. We find no difference of the Mo–sulfido bond lengths between the SRED, SPVM, SVPP, SBEN, and SASX sulfido derivatives which have single bonds of 2.4 Å bond length. This bond shrinks to 2.2 Å when sulfurated crystals are transferred into sulfide-free buffer in SOXY and SOX3 crystals. At the same time part of the sulfur is hydrolyzed and replaced by on oxo group, pointing to an extreme lability of the sulfido group.

There is evidence by extended x-ray absorption fine structure (EXAFS) for an oxo group in both oxidized and reduced forms of xanthine oxidase and for three sulfur ligands, with two long and one short bond in oxidized enzyme and three long bonds in reduced enzyme. However, evidence by EXAFS for a second oxygen ligand, which we now locate and identify as coordinated water, is weak (19, 20).

The oxidized form of ANE may have a partial disulfide bond of the dithiolene group as had been discussed for a MoVI cysteamine derived complex with a S—S bond of 2.76 Å (21). These authors suggest that the dithiolene group may participate in the MoVI → MoIV redox process to involve a disulfide–thiolate interconversion associated with formal oxidation state changes of the metal. Given the increase in S—S distance and increased dithiolene puckering observed here upon reduction of Mop, it is likely that a comparable phenomenon is seen in the enzyme as well.

EPR and EXAFS measurements have been interpreted as an oxo, sulfido coordination, MoVI, ═O, ═S of the functional, oxidized form of xanthine oxidase and a MoVI═O, —SH structure in the reduced MoIV state. In further refinement, including determination of the ^{17}O hyperfine coupling, the resting form of xanthine oxidase was formulated as *fac* [MoVI═O, ═S, —(OH)] (22). The complex of reduced enzyme with violapterin (the product of the enzyme's action on lumazine) was studied by resonance Raman measurements, and the latter was interpreted as a charge-transfer complex between the molybdenum center and the product directly coordinated via its 7-hydroxyl group to the molybdenum (23). The lack of resonance enhancement of the Mo═O stretching mode was interpreted as reflecting location of the oxo group "cis" to the bound product. These suggestions are essentially consistent with the structure described here as *fac* [Mo═O(MOH1), —S(MOH3), —OH_2(MOH2)], assuming that

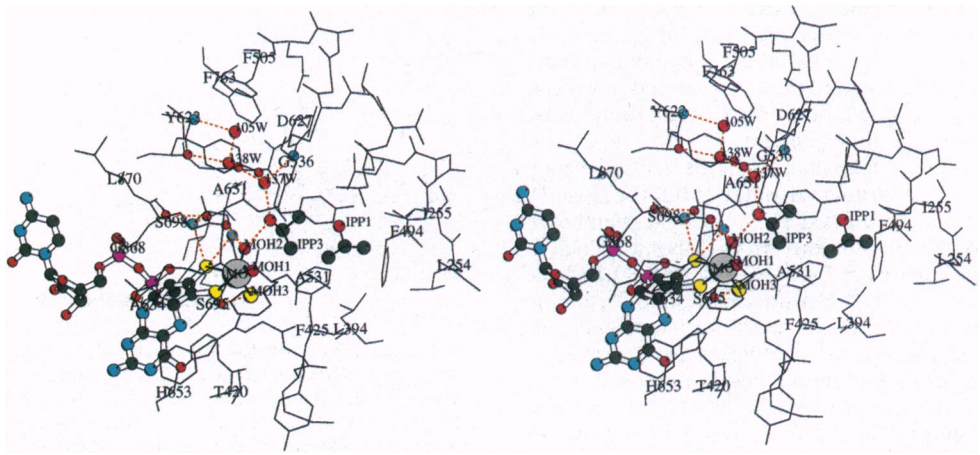

FIG. 4. Atomic model of the molybdopterin cytosine dinucleotide in Mop, the molybdenum and its ligands, the two isopropanol molecules IPP1 (outer site), IPP3 (inner site), the internal water chain 105W, 138W, 137W, and the protein environment. Hydrogen bonds involving the molybdenum ligands, IPP3, Glu-869, and the internal water molecules are drawn as red broken lines.

the coordinated water is replaced by the substrate/product ligand.

Water MOH2 is indeed the metal ligand most accessible from the substrate tunnel and most likely the source of the transferred hydroxo group (24) and the binding site of reaction intermediates. It is hydrogen-bonded to Glu-869 (probably as donor) and to the hydroxyl-group of isopropanol IPP3. The methyl groups of isopropanol are in hydrophobic contact with Phe-425, Tyr-535, Leu-497, and Leu-626. We suggest the isopropanol site as a model of the Michaelis complex of an aldehyde substrate, whereby the carbonyl oxygen of substrate replaces the hydroxyl group of isopropanol and the hydrogen is in place of the $C^{\delta 1}$ methyl group directed toward the metal site. In this configuration the carbonyl oxygen would accept two hydrogen bonds from molybdenum-bound water MOH2 and water 137W to polarize it and thereby facilitate nucleophilic attack at the carbonyl carbon by MOH2.

This suggestion is supported in general by the observation that alcohols are substrate-analog inhibitors of Mop (12) and xanthine oxidase (see ref. 25). Ethylene glycol is a slow substrate of xanthine oxidase (26) and EPR measurements of xanthine oxidase inhibited with methanol and formaldehyde yield identical "inhibited" signals (27) in accord with similar binding modes for alcohols and aldehydes. Specifically, substrate binding in the second coordination sphere of the molybdenum in the Michaelis complex is supported by the absence in xanthine oxidase of proton coupling in the "rapid type 1" EPR signal due to the C-8-bound proton of the slowly reacting substrate 2-hydroxy-6-methylpurine (28) (coupling occurs only after substrate oxidation and hydride transfer), by the interaction of 8-bromoxanthine (a strong inhibitor of xanthine oxidase) in a way that is typical of purine substrates (29) with a Mo-Br distance greater than 4 Å (30), and by the binding of arsenite to the metal which forms a first coordination sphere complex without interfering with binding of substrates (31).

The suggested structure of the Michaelis complex offers a simple pathway for the chemical transformation whereby nucleophilic attack at the carbonyl carbon by MOH2 and hydride transfer from it to the sulfido group may occur, generating the carboxylic acid product bound to the metal via the transferred oxygen. The water MOH2 nucleophile is transferred as OH^- (after proton transfer to its associated base Glu-869) over a distance estimated to be ≈3.4 Å. Bond formation requires further approach, whereby the carbonyl oxygen may remain anchored by its hydrogen bond to 137W. This would bring the aldehydic hydrogen closer to the sulfido group (MOH3) for transfer to occur. The transferred hydrogen from the substrate is observed as the proton strongly coupled to the molybdenum in the rapid type 1 EPR signal (32–34). The sulfhydryl hydrogen may indeed be closer than 2.5 Å to the metal. Other close protons at, or derived from, the ligand water MOH2 are further away with 2.6 Å and 2.9 Å and one of these may represent the second coupled proton observed in various EPR-active species (35, 36). No other protons are found close enough to couple with the molybdenum.

The aldehyde group is coplanar with the sulfido group (MOH3), Mo, and the coordinated water (MOH2) (Fig. 3), such that the educt may be viewed as an open six-membered ring oriented perpendicular to the Mo=O bond, which is transformed into product by a 1,6 (—C—H → S=) hydride shift and a 1,3 (O=C ← OH_2) trans-annular bond formation assisted by metal-centered molecular orbitals (molecular orbital energy level diagrams of Mo complexes are described in ref. 37). A close carbon metal interaction is proposed in the "inhibited" species of xanthine oxidase by electron nuclear double resonance studies (38). The presence of product or product analogs bound to the reduced MoIV center of these enzymes is also supported by EXAFS (19, 20) and resonance Raman studies (39). In addition, a Hammett analysis of quinazoline hydroxylation catalyzed by xanthine oxidase (40–42) is consistent with a mechanism involving nucleophilic attack on substrate by a metal coordinated OH^-.

There is kinetic evidence that substrate binding (43) and product release from the reduced enzyme (44) are two-step processes. These we associate with binding at the outer isopropanol binding site (IPP1) as a pre-Michaelis complex and transfer to the inner compartment (IPP3) in a kinetically distinct step to form the Michaelis complex (Fig. 4). Binding of substrate in the outer compartment (IPP1 site) may explain substrate inhibition observed for Mop (12) and xanthine oxidase (40, 45) when release of product through the "swinging doors" formed by Leu-394, Phe-425, Phe-494, Leu-497, and Leu-626, which separate inner and outer compartments, are blocked by waiting substrate molecules. We also suggest the outer, very spacious compartment as the binding site of voluminous inhibitors of xanthine oxidase (46).

Release of the carboxylic acid product from the molybdenum site may be facilitated by transient binding of Glu-869 to the metal to maintain penta-coordination. The molybdenum water site may then be refilled by the chain of internal water molecules of which two, 137W and 138W, display four hydrogen bonds, whereas the innermost 105W has only two being located in a very apolar environment of Phe-505, Phe-763, Tyr-622. These molecules constitute a column of water molecules able to replenish the vacant MOH2 site.

The reaction for the reductive half-cycle as outlined above is shown in Fig. 5. It resembles earlier proposals (2), but provides the exact stereochemical relationships and differs by suggesting a water ligand, not the oxo group, as the labile oxygen to be transferred onto the substrate as had also been indicated by electron nuclear double resonance and kinetic studies of xanthine oxidase (47). It operates with minimal structural changes at the molybdenum site during turnover. A kinetically competent MoV state giving rise to the "very rapid" EPR signal is known to possess strongly coupled sulfur and oxygen and weakly coupled carbon but no coupling to exchangeable protons (2, 31, 48). These observations suggest a structure b′ similar to b after transfer of an electron to the iron redox centers and ionization of the S–H proton. Other species with MoV centers exhibiting "rapid" EPR

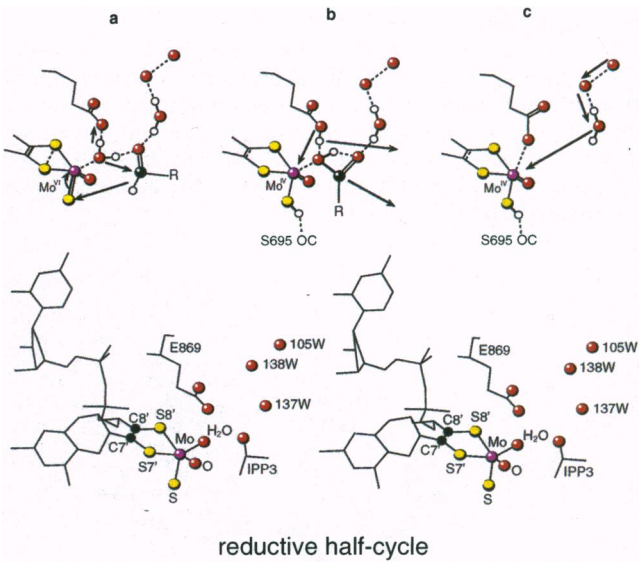

FIG. 5. The reductive half-cycle of the hydroxylation reaction of Mop and xanthine oxidase. (*Lower*) Stereo representation of the observed molybdenum cofactor with bound isopropanol IPP3. (*Upper*) Hypothetical structures of *a*, the Michaelis complex with MoVI and aldehyde substrate; *b*, the enzyme carboxylic acid product complex with MoIV; and *c*, an intermediate after product dissociation, in which Glu-869 is bound to the metal. Increased electron density between the dithiolene sulfurs in the oxidized state and decreased electron density in the C=C double bond in the reduced state are indicated.

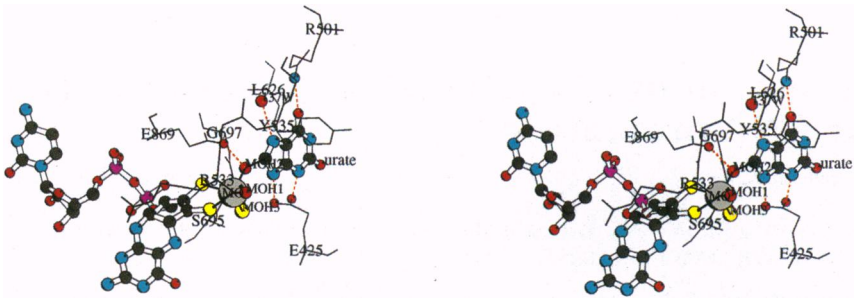

FIG. 6. Model of a hypothetical urate complex. Phe-425 in Mop has been exchanged for Glu in xanthine oxidase.

signals are "off pathway" intermediates (49, 50) and may represent variants of structure b.

The SASX data set shows arsenite bound at the IPP3 site. Arsenic is very close to the molybdenum according to EXAFS data (51) and believed to be covalently attached to the sulfido group. It has strong effects on the MoV EPR signal (52–54). The crystal structure does not represent this model, but may be a Michaelis complex unable to proceed to the covalent adduct by the reaction conditions in the crystal.

The urate–MoIV complex of xanthine oxidase has been modeled as a *fac* (MoIV, ═O, —SH, —O—urate) complex. Residue Phe-425 in Mop has been exchanged for the homologous Glu in xanthine oxidase. The glutamate is well positioned to bind to the N3, N9 amidinium substructure of a purine (Fig. 6) and water 137W is suggested as the specific recognition site for N7. The imidazole portion of a purine ligand cannot exactly replace the isopropanol of an aldehyde-like Michaelis complex, but may be accomodated by small shifts.

Nucleophilic addition of a metal activated water to an electrophilic center has precedence with hydrolytic enzymes, carboxypeptidase A and B (55, 56) and collagenases (57). The metal is zinc in these enzymes, but the proton abstracting base is also a glutamate in a steric arrangement resembling Mo-MOH2-Glu-869 in Mop. C-8 of a purine is susceptible to nucleophilic attack when N-7 is protonated. An appropriate proton donor in the case of Mop is water 137W. This is in close analogy to GTP cyclohydrolase where nucleophilic attack by a water at C-8 of the guanine (with following cleavage of the C-8 N-9 bond) is facilitated by a histidine residue hydrogen bonded to N-7 (58).

We thank R. C. Bray (Brighton) and A. Xavier (Oeiras) for discussions, the staff of the UGA Fermentation Plant for growing the cells (J.L.), M. J. Almendra for functional studies (J.J.G.M. and I.M.), and M. Schneider for help with the calculations and plots (R.H. and P.H.). This work was supported by a Junta Nacional de Investigacão Científica e Tecnológica–Bundesministerum für Forschung und Technik project (M.A., M.J.R., and R.H.), by a PRAXIS/BD/2795/94 Ph.D. grant (M.A.), and by the AvHumboldt Foundation (M.J.R.).

1. Stiefel, E. I. (1993) *ACS Symp.* **535,** 1–22.
2. Hille, R. (1993) *ACS Symp.* **535,** 22–38.
3. Enemark, J. H. & Young, C. G. (1993) *Adv. Inorg. Chem.* **40,** 1-88.
4. Thoenes, U., Flores, O. L., Neves, A., Devreese, B., VanBeumen, J. J., Huber, R., Romao, M. J., LeGall, J., Moura, J. J. G. & Rodrigues-Pousada, C. (1994) *Eur. J. Biochem.* **220,** 901–910.
5. Romão, M. J., Archer, M., Moura, I., Moura, J. J. G., LeGall, J., Engh, R., Schneider, M., Hof, P. & Huber, R. (1995) *Science* **270,** 1170–1176.
6. Romão, M. J., Barata, B. A. S., Archer, M., Lobeck, K., Moura, I., Carrondo, M. A., LeGall, J., Lottspeich, F., Huber, R. & Moura, J. J. G. (1993) *Eur. J. Biochem.* **215,** 729–732.
7. Leslie, A. G. W. (1990) MOSFLM Program (Crystallographic Computing School, Bischenberg, Germany).
8. Collaborative Computational Project No. 4 (1994) *Acta Crystallogr. D* **50,** 760–763.
9. Brünger, A. T. (1990) X-PLOR Version 2.1 Manual (Yale Univ. Press, New Haven, CT).
10. Engh, R. & Huber, R. (1991) *Acta Crystallogr. A* **47,** 392–400.
11. Jones, T. A. (1978) *J. Appl. Crystallogr.* **11,** 268–272.
12. Barata, B. A. S., LeGall, J. & Moura, J. J. G. (1993) *Biochemistry* **32,** 11559–11568.
13. Malthouse, J. P. G. & Bray, R. C. (1980) *Biochem. J.* **191,** 265–267.
14. Massey, V. & Edmondson, D. (1970) *J. Biol. Chem.* **245,** 6595–6598.
15. Wahl, R. C. & Rajagopalan, K. V. (1982) *J. Biol. Chem.* **257,** 1354–1359.
16. Morpeth, F. F. & Bray, R. C (1984) *Biochemistry* **23,** 1332–1338.
17. Turner, N., Barata, B., Bray, R., C., Deistung, J., LeGall, J. & Moura, J. G. (1987) *Biochem. J.* **243,** 755–761.
18. Barata, B. A. S., Liang, J., Moura, I., LeGall, J., Moura, J. J. G. & Hanh Huynh, B. (1992) *Eur. J. Biochem.* **204,** 773–778.
19. Hille, R. George, G. N., Eidsness, M. K. & Cramer, S. P. (1989) *Inorg. Chem.* **28,** 4018–4022.
20. Turner, N. A., Bray, R. C. & Diakun, G. P. (1989) *Biochem J.* **260,** 563–571.
21. Stiefel, E. I., Miller, K. F., Bruce, A. E., Corbin, J. L., Berg, J. M. & Hodgson, K. O. (1980) *J. Am. Chem. Soc.* **102,** 3624–3626.
22. Greenwood, R. J., Wilson, G. L., Pilbrow, J. R. & Wedd, A. G. (1993) *J. Am. Chem. Soc.* **115,** 5385–5392.
23. Oertling, T. A. & Hille R. (1990) *J. Biol. Chem.* **265,** 17446–17450.
24. Hille, R. & Sprecher, H. (1987) *J. Biol. Chem.* **262,** 10914–10917
25. Bray, R. C. (1980) in *Biological Magnetic Resonance*, eds. Reuben, J. & Berliner, L. J. (Plenum, New York), Vol. 2, pp. 45–84.
26. Tanner, S. J. & Bray, R. C. (1978) *Biochem. Soc. Trans.* **6,** 1331–1333.
27. Pick, F. M., McGartoll, M. A. & Bray, R. C. (1971) *Eur. J. Biochem.* **18,** 65–72.
28. Hille, R., Jong, H. K. & Hemann, C. (1993) *Biochemistry* **32,** 3973–3980.
29. Hille, R. & Stewart, R. C. (1984) *J. Biol. Chem.* **259,** 1570–1576.
30. Cramer, S. P. & Hille, R. (1985) *J. Am. Chem. Soc.* **105,** 8164–8169.
31. Hille, R. & Massey, V. (1985) in *Molybdenum Enzymes*, ed. Spiro, T. G. (Wiley, New York), pp. 443–518.
32. Bray, R. C. & George, G. N. (1985) *Biochem. Soc. Trans.* **13,** 560–567.
33. Gutteridge, S., Tanner, S. J. & Bray, R. C. (1978) *Biochem. J.* **175,** 869–878.
34. Gutteridge, S., Tanner, S. J. & Bray, R. C. (1978) *Biochem. J.* **175,** 887–897.
35. Bray, R. C. & Gutteridge, S. (1982) *Biochemistry* **21,** 5992–5999.
36. Bray, R. C. (1980) in *Biological Magnetic Resonance*, eds. Berliner, L. J. & Reuben, J. (Plenum, New York), Vol. 2, pp. 45–84.
37. Carducci, M. D., Brown, C., Solomon, E. I. & Enemark, J. H. (1994) *J. Am. Chem. Soc.* **116,** 11856–11868.
38. Howes, B. D., Bennet, B., Bray, R. C., Richards, R. L. & Lowe, D. J. (1994) *J. Am. Chem. Soc.* **116,** 11624–11625
39. Oertling, W. A. & Hille, R. J. (1990) *J. Biol. Chem.* **265,** 17446–17450.
40. Skibo, E. B., Gilchrist, J. H. & Chang, H. L. (1987) *Biochemistry* **26,** 3032–3037.
41. Hofste, B. H. J. (1955) *J. Biol. Chem.* **216,** 235–244.
42. D'Ardenne, S. C. & Edmondson, D. E. (1990) *Biochemistry* **29,** 9046–9052
43. Hille, R. & Stewart, R. C. (1984) *J. Biol. Chem.* **259,** 1570–1576.
44. Davis, M. D., Olsen, J. S. & Palmer G. (1984) *J. Biol. Chem.* **259,** 3526–3533.
45. Morpeth, F. F. (1983) *Biochim. Biophys. Acta* **744,** 328–334.
46. Okamoto, K. & Nishino, T. J. (1995) *J. Biol. Chem.* **270,** 7816–7821.
47. Howes, B. D., Bray, R. C., Ricards, R. L., Turner, N. A., Bennet, B. & Lowe, D. J. (1996) *Biochemistry* **35,** 1432–1443.
48. Bray, R. C. (1988) *Q. Rev. Biophys.* **21,** 299–329.
49. Jong, H. K. & Hille, R. (1993) *J. Biol. Chem.* **268,** 44–51.
50. Hille, R., Jong, H. K. & Hemann, C. (1993) *Biochemistry* **32,** 3973–3980.
51. Cramer, S. P. & Hille, R. (1985) *J. Am. Chem. Soc.* **107,** 8164–8169.
52. George, G. N. & Bray, R. C. (1983) *Biochemistry* **22,** 1013–1021.
53. Hille, R., Stewart, R. C., Fee, J. A. & Massey, V. (1983) *J. Biol. Chem.* **258,** 4849–4851.
54. Howes, B. D., Pinhal, N. M.,Turner, N. A., Bray, R. C., Anger, G., Ehrenberg, A., Raynor, J. B. & Lowe, D. J. (1990) *Biochemistry* **29,** 6120–6127.
55. Guasch, A., Coll, M., Aviles, F. X. & Huber, R. (1992) *J. Mol. Biol.* **224,** 141–157.
56. Phillips, M. A., Fletterick, R. & Rutter, W. J. (1990) *J. Biol. Chem.* **265,** 20692–20698.
57. Grams, F., Reinemer, P., Powers, J. C., Kleine, T., Pieper, M., Tschesche, H., Huber, R. & Bode, W. (1995) *Eur. J. Biochem.* **228,** 830–841.
58. Nar, H., Huber, R., Auerbach, G., Fischer, R., Hösl, C., Ritz, H., Bracher, A., Meining, W., Eberhardt, S. & Bacher, A.(1995) *Proc. Natl. Acad. Sci. USA* **92,** 12120–12125.